Characterization of embedded fiber optic strain sensors into metallic structures via ultrasonic additive manufacturing

John J. Schomer[a], Adam J. Hehr[a], and Marcelo J. Dapino[a]

[a]NSF I/UCRC on Smart Vehicle Concepts, Department of Mechanical and Aerospace Engineering, The Ohio State University, 201 W 19th Ave. Columbus, Ohio 43210

ABSTRACT

Fiber Bragg Grating (FBG) sensors measure deviation in a reflected wavelength of light to detect in-situ strain. These sensors are immune to electromagnetic interference, and the inclusion of multiple FBGs on the same fiber allows for a seamlessly integrated sensing network. FBGs are attractive for embedded sensing in aerospace applications due to their small noninvasive size and prospect of constant, real-time nondestructive evaluation. In this study, FBG sensors are embedded in aluminum 6061 via ultrasonic additive manufacturing (UAM), a rapid prototyping process that uses high power ultrasonic vibrations to weld similar and dissimilar metal foils together. UAM was chosen due to the desire to embed FBG sensors at low temperatures, a requirement that excludes other additive processes such as selective laser sintering or fusion deposition modeling. In this paper, the embedded FBGs are characterized in terms of birefringence losses, post embedding strain shifts, consolidation quality, and strain sensing performance. Sensors embedded into an ASTM test piece are compared against an exterior surface mounted foil strain gage at both room and elevated temperatures using cyclic tensile tests.

Keywords: Fiber Bragg grating (FBG), ultrasonic additive manufacturing (UAM), structural health monitoring, embedded sensing

1. INTRODUCTION

Structural health monitoring plays an important role in modern engineering by reducing excess safety factors, detecting damage prior to failure, and allowing for efficient system maintenance. The increasing demand for robust structural condition detection is driving the need for solutions in which sensors, and potentially electronic components, are embedded into structures. Embedded sensing allows for the measurement of mechanical signals within parts that cannot be easily monitored externally, such as curved beams, aircraft wings, and turbine blades. Embedded sensing also meets requirements in structures subjected to harsh or extreme conditions, such as corrosive environments or applications which experience extreme temperatures, where external sensors cannot survive. Sensors are typically embedded during the fabrication of a component, often in between ply layers of laminated composites.[1,2] However, advancements in additive manufacturing enable the embedment of sensing elements into plastic and metal components. Fiber Bragg Grating (FBG) sensors consist of a glass core with a written grating, a glass cladding, and an external protective coating. FBGs are used in embedded sensing applications such as composite pressure vessels, composite lap joints, and composite manufacturing processes, and show promise for being embedded into monolithic metal structures.[3]

FBG sensors are used for real-time in-situ measurement of strain and temperature. When white light is sent through the fiber by an interrogator, a specific wavelength is reflected. This wavelength is determined by the spacing between individual gratings, which are written into the fiber via an UV laser.[4] Figure 1 shows that when the distance between gratings changes as a result of either mechanical or thermal strain, a measureable change in reflected wavelength occurs. Since FBG sensing networks are based on measuring light, they are immune to electromagnetic interference. FBG sensors have potential uses in high-temperature strain sensing applications due to the high melting point of silica glass (over 1000 degrees Celsius).[5] By incorporating multiple gratings

Further author information: (Send correspondence to M.J. Dapino)
M.J.D.: E-mail: dapino.1@osu.edu, Telephone: 1 614 688 3689
J.J.S.: E-mail: schomer.11@buckeyemail.osu.edu

Sensors and Smart Structures Technologies for Civil, Mechanical, and Aerospace Systems 2016, edited by Jerome P. Lynch, Proc. of SPIE Vol. 9803, 980320 · © 2016 SPIE
CCC code: 0277-786X/16/$18 · doi: 10.1117/12.2219690

Downloaded From: http://proceedings.spiedigitallibrary.org/ on 07/12/2017 Terms of Use: http://spiedigitallibrary.org/ss/termsofuse.aspx

with different spacing on a single fiber, known as multiplexing, multiple wavelengths of light can be reflected, allowing for strain sensing at different points in a structure with the same interrogator. This allows for a complex sensing network to be incorporated via the integration of a single fiber into a structure.

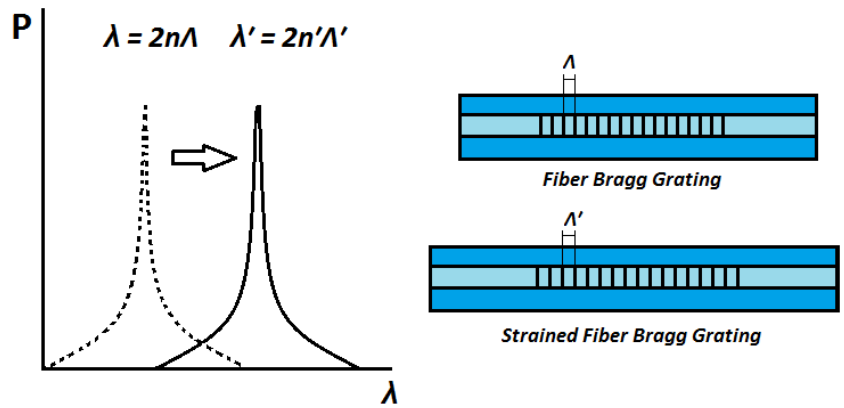

Figure 1. FBG sensing: as the FBG is strained, the grating spacing increases, and an associated change in reflected wavelength takes place.

Although FBG sensors are most effective when directly built into plastic and metallic components for health monitoring, their brittleness rules out conventional manufacturing methods that involve fusion of the matrix material.[6] Additive manufacturing, or 3D printing, is the method of adding material to fabricate a part rather than removing material, and offers unprecedented opportunities in the creation of smart structures,metal-matrix composite materials, and parts with complex internal geometries. Instead of inserting an FBG sensor into a previously finished part or a composite, the part can be built around the existing sensor, resulting in a single piece plastic or metal structure with integrated sensing. Fused deposition modeling is a 3D printing method that outputs plastic parts, and is capable of incorporating FBGs. FBGs have been embedded though this process in order to measure residual stresses in parts after fabrication.[7] FBGs were also embedded into a polymeric sample made through selective laser sintering, an additive process in which powders are fused via a laser, and comparative strain measurements were taken from the FBG, an extensometer, and an externally mounted foil gage.[8] In the latter study, the sintering process temperatures were high enough to cause degradation of acrylate coated FBGs.

Embedding FBG sensors into metallic components is challenging due to the effects of thermal strain on the sensor during fabrication, coating degradation that occurs at elevated temperatures, and polarization losses induced by uneven cross-sectional loading of the fiber. Through the use of selective laser melting, FBGs were embedded into a stainless-steel part in order to measure the residual strain from the process, but fabrication issues led to polarization errors and voids between the matrix material and the sensor.[9] A metal based additive manufacturing technique that has successfully built FBG sensors into parts is ultrasonic additive manufacturing (UAM). UAM uses a sonotrode to apply force and high power ultrasonic vibrations, generated by piezoelectric transducers, to metal foils in order to weld similar and dissimilar metal foils.[10] UAM is a solid-state welding process which allows for the inclusion of subtractive operations during builds. Unlike other additive processes, UAM welds occur with little heat generation, allowing for the embedding of sensing elements near room temperature. Previous studies on the use of UAM to embed optical fiber have focused on successful embedding of non-graded fiber into an aluminum matrix, reducing damage to the fiber, and thermomechanical response testing of FBGs. These studies were able to transmit light through embedded fibers, embed multiplexed FBGs into aluminum, and measure residual strain on the FBGs resulting from the UAM process.[11,12]

This study seeks to provide an experimental characterization of FBG sensors embedded into aluminum 6061. Due to possible cross-sectional loading, residual strain, and poor mechanical coupling, it is necessary to obtain comparative strain measurements in order to validate the embedded FBG sensors. In contrast to the previous

Downloaded From: http://proceedings.spiedigitallibrary.org/ on 07/12/2017 Terms of Use: http://spiedigitallibrary.org/ss/termsofuse.aspx

UAM studies where the FBG sensors used were electroplated prior to consolidation, the FBGs in this study were embedded using their commercially available external coatings. FBG sensor peformance was evaluated based on ASTM tensile testing, dynamic response, birefringence profile, and sample microscopy. Thermal limits on embedded FBG sensing capability were quantified. The findings of this study provide a basis for motivating FBG measurements in metal components fabricated by the UAM process over a wide range of conditions.

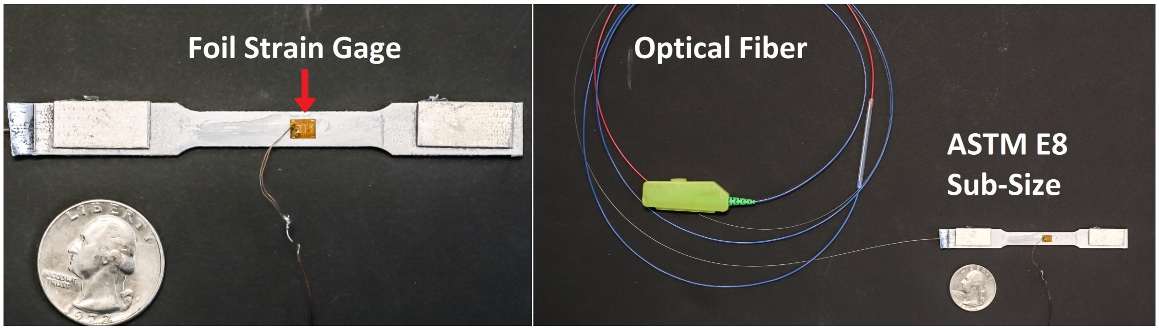

Figure 2. example of a subsize tensile test specimen with embedded FBG sensor fabricated via UAM.

2. EXPERIMENTAL METHODS

2.1 Fabrication Procedures

Optical fiber containing FBG sensors were embedded into an aluminum 6061 matrix via UAM. In UAM, ultrasonic scrubbing action induces plastic deformation between the foils and baseplate material, dispersing the oxide layers and creating a bond through metal-to-metal contact. This bond forms near room temperature and does not melt the foil. The inclusion of periodic machining operations allows for material to be placed inside of channels prior to encapsulation. The test specimens produced for this study were based on ASTM E8 standards (Figure 2),[13] and were produced on a Fabrisonic SonicLayer 4000 (Figure 3).

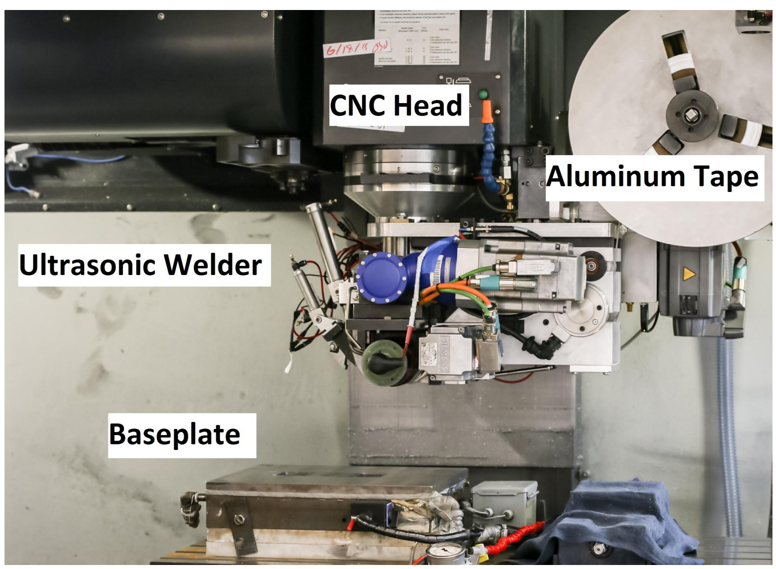

Figure 3. commercial 9 kW UAM system, Fabrisonic SonicLayer 4000.

The FBG sensors used were written onto 125 micron diameter standard single mode fibers, with reflected nominal wavelengths of 1550 nm. The sensors were coated in either acrylate (PMMA) or polyamide (PI) for

Downloaded From: http://proceedings.spiedigitallibrary.org/ on 07/12/2017 Terms of Use: http://spiedigitallibrary.org/ss/termsofuse.aspx

mechanical protection. Several fabrication parameters impact the performance of embedded FBGs, including the amplitude, speed, and down force on the sonotrode.[10,14] Samples were built using 0.154 mm (6 mil) thick foil, 4000 N down force, ultrasonic amplitude of 32 microns, and a weld speed of 508 cm/min (200 in/min). Two to three layers of foil were welded onto an aluminum baseplate prior to embedment of the fiber, to ensure consistent properties of the matrix material surrounding the fiber. A channel of 0.254 mm (10 mil) depth and equal width was then cut lengthwise across the surface sample using a ball-tipped end mill, and the FBG was positioned manually in the center of the test specimen. After temporarily securing the fiber, an encapsulating layer of aluminum foil was welded over the fiber. The ASTM E8/subsize E8[13] sample shape was then traced using a 3.175 mm (1/8th in) end mill, and the excess baseplate material was removed from the sample using the CNC features of the SonicLayer 4000.

2.2 Birefringence

Measurement inconsistency due to birefringence, the dependence of the refractive index on the orientation of the fiber, was analyzed.[15] Cross sectional deformation of the core and cladding leads to an increase in the birefringence effects on the fiber.[16] Deformations on the order of picometers from uniform fiber cross-section lead to errors in FBG strain measurements. Optical detection of such small deformations is prohibitively difficult, so the direct measurement of the FBGs response to polarized light is required to ensure acceptable performance. Birefringence data was obtained by manually polarizing the light signal through the use of a polarization controller (Figure 4) supplied by Insensys Ltd. This polarization controller induces birefringence in the connecting fiber optic cable between the FBG interrogator and the FBG sensor. In this manner, the FBG sensors are characterized over a wide range of signal polarizations.

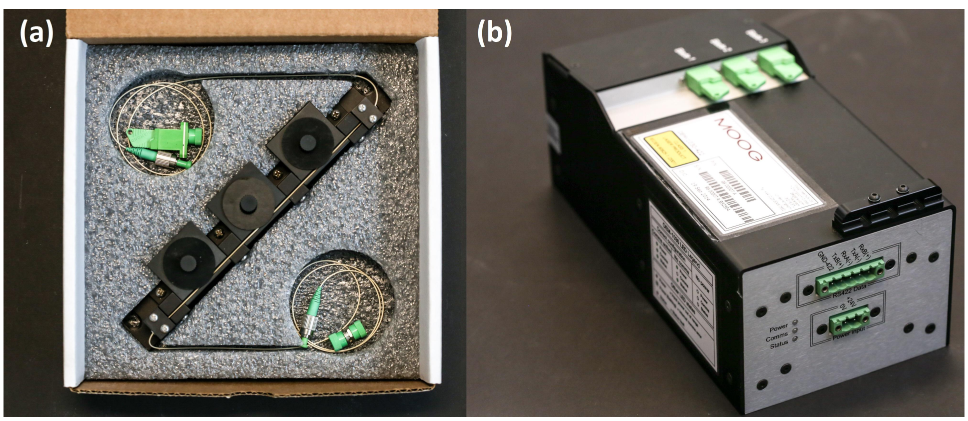

Figure 4. fiber Bragg grating test equipment: (a) polarization Controller (b) FBG interrogator.

2.3 Physical Testing

Cantilever bending testing was performed to investigate the dynamic response and bandwidth of the FBG sensors by clamping the test specimens at one end. Tensile test characterization was performed on a TestResources load frame, and data acquisition was handled by a National Instruments DAQ unit. The FBGs were measured using an interrogator supplied by Moog Inc, which exported analog data to the NI DAQ. This was done to ensure that all values were measured on the same time signal, allowing for direct comparison of strain, temperature, and tensile load values. Vishay foil strain gages were mounted on the surface of test specimens, and were used as a comparative benchmark for sensor performance. The foil gages used to examine the effects of thermal loading on embedded FBG performance are thermally invariant with aluminum.

2.4 Thermal Characterization

Samples were heated in an oven while under no tensile or compressive load in an effort to obtain their maximum operating temperature. FBG strain data was collected and compared to the coefficient of thermal expansion

Downloaded From: http://proceedings.spiedigitallibrary.org/ on 07/12/2017 Terms of Use: http://spiedigitallibrary.org/ss/termsofuse.aspx

(CTE) of aluminum. The temperature at which the sensors no longer tracked the CTE of Aluminum was taken to be the operational temperature limit of the embedded FBGs, as this divergence implies the breakdown of the coupling between the sensor and Aluminum matrix. Full-size tensile test specimens were tested in a load frame with integrated furnace, shown schematically in Figure 5. Temperature measurements were taken in real time from K-type thermocouples. The FBGs were also tested for inscription reversal, which is the breakdown of the grating caused by exposure to elevated temperatures.

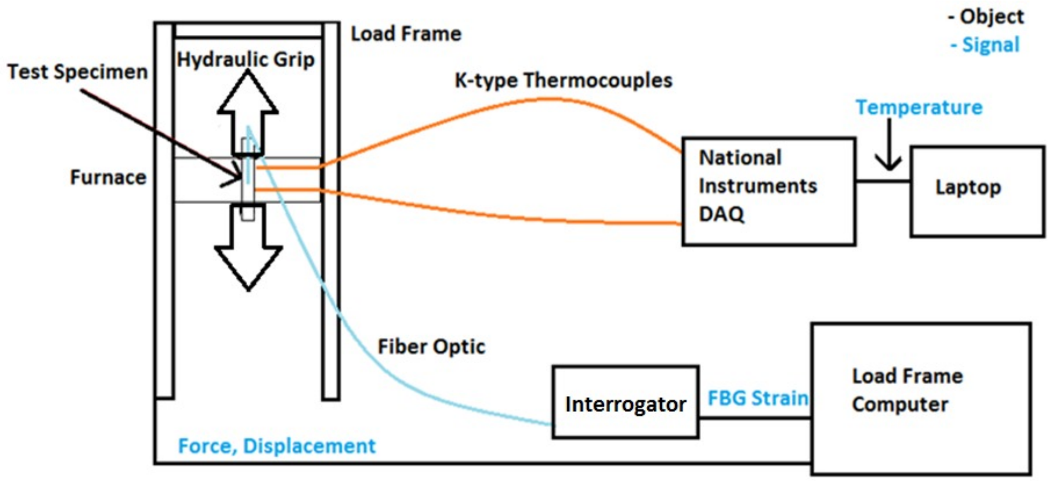

Figure 5. schematic for high temperature tensile testing.

3. RESULTS AND DISCUSSION

3.1 Birefringence

The signal response to polarization of light is caused by cross-sectional deformation of the core and cladding of the fiber. A sensor with poor birefringence response can yield significant errors in reported strain values, on the order of 60-100 microstrain. For this study, the birefringence was investigated by use of a polarization controller, which serves to send a wide range of polarized signals into the fiber to induce errors. A poor FBG with cross sectional deformation was supplied by Insensys and used as a reference, characterized by a total shift in Delta Wavelength of more than 0.06 nanometers when a polarized signal is passed through the mechanically unloaded FBG (Figure 6(a)). No significant birefringence effects were experienced by the fiber when embedded with proper channel height (Figure 6(b)). If the FBGs are placed in a loaded configuration, they see an increase in losses due to birefringence, regardless of the type of external protective coating. Conversely, the presence of a channel allows the fiber to be 'unloaded' by the welder, and in all cases minimizes the birefringence. FBGs embedded in the 'unloaded' configuration often see less than a 0.01 total wavelength change in response to polarized light. FBGs embedded in a curved configuration also saw no change in birefringence response.

Downloaded From: http://proceedings.spiedigitallibrary.org/ on 07/12/2017 Terms of Use: http://spiedigitallibrary.org/ss/termsofuse.aspx

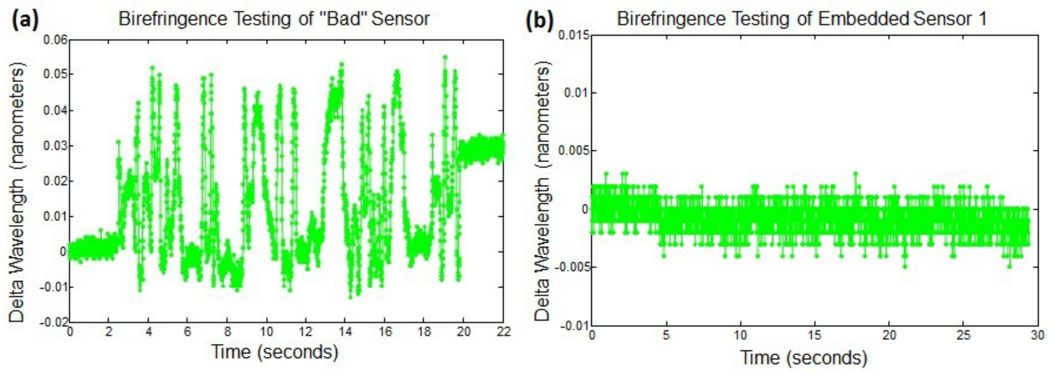

Figure 6. response to polarization of FBGs: (a) Reference 'poor' sensor supplied by Insensys; (b) Acrylate coated sensor after embedment into aluminum.

3.2 Cantilever Bending

Test specimens were clamped in place during cantilever bend testing to verify the FBG strain profile in comparison to the foil gage profile. Due to the sensors' proximity to the neutral axis (Figure 7(a)), the data was scaled so that the strain profile was more visible (Figure 7(b)). Manual quasi-static bending was induced in the sample, as well as a flick test to obtain the impulse response. Frequency content analysis in the form of a Fast Fourier Transform demonstrates aliasing occurring in the FBG signal, which will need to be filtered out in future applications, but otherwise confirms the harmonic motion observed by the foil gage.

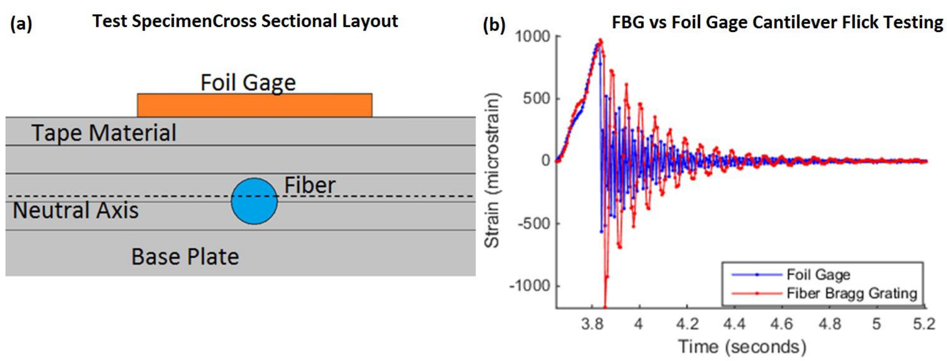

Figure 7. cantilever testing: (a) test specimen cross section; (b) FBG response to impulse input.

3.3 Cyclic Tensile Testing

The FBG sensors were found to trace the profile demonstrated by the foil gages with a high level of accuracy during quasi-static cyclic load testing. The primary sources of error are variation due to temperature shifts and slippage. At elevated temperatures, the shifting temperature and thermal strain on the specimen lead to measured changes in the FBG sensors (Figure 8(a)-(b)). Slippage was most pronounced during tensile testing in the polyamide coated fibers, as shown by the presence of hysteresis curves in the low frequency cyclic loading (Figure 8(c)-(d)). In contrast, the acrylate coated sensors are consistent with the foil strain gages, and failed prior to the sample at 4537 microstrain (Figure 8(e)-(f)). The presence of slip in the polyamide fibers is supported by the stress in the aluminum matrix being significantly below the yield stress, as confirmed by the failure of the aluminum matrix prior to the optical fiber (Figure 9).

Downloaded From: http://proceedings.spiedigitallibrary.org/ on 07/12/2017 Terms of Use: http://spiedigitallibrary.org/ss/termsofuse.aspx

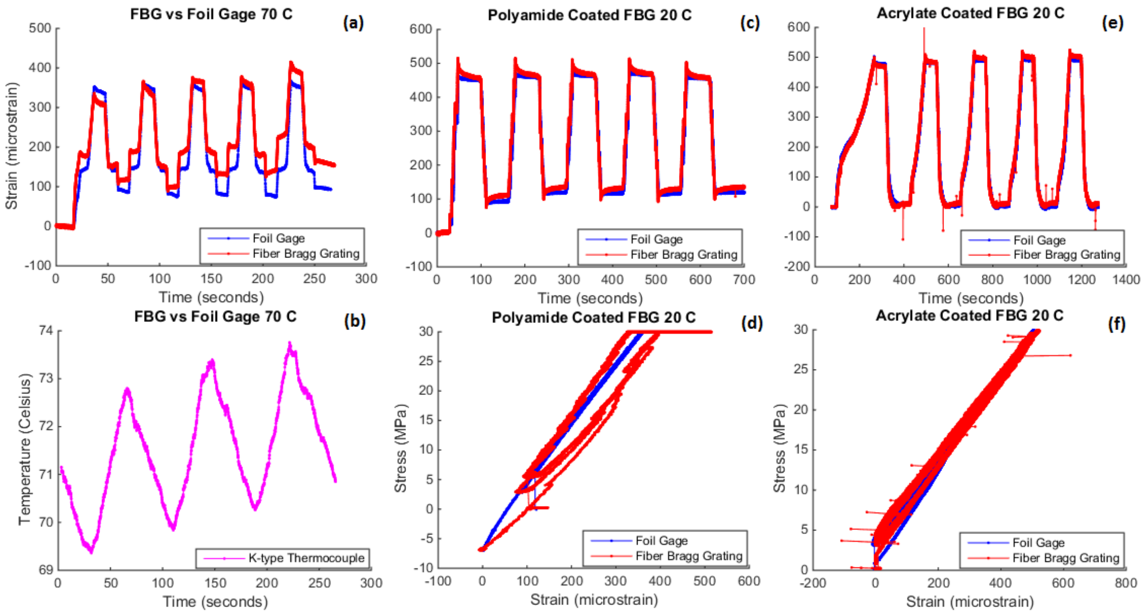

Figure 8. cyclic testing of FBG sensors: (a) tensile testing at 70 Celsius shows drift in FBG measured values from foil gage values; (b) temperature profile of the 70 Celsius test shows uniform fluctuation in temperature which matches the discrepancy in observed strain values; (c) room temperature quasi-static cyclic testing of polyamide coated FBG; (d) stress-strain profile shows evidence of hysteresis in FBG measurements but not in foil gage; (e) room temperature tensile testing of Acrylate coated FBG; (f) stress-strain profile does not show evidence of hysteresis present in either sensor.

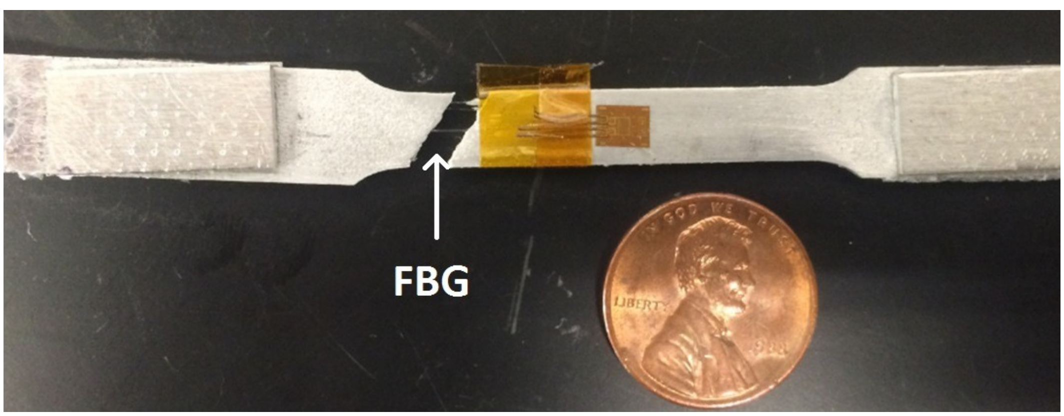

Figure 9. polyamide coated sensor surviving despite failed aluminum matrix.

3.4 Microscopy

Cross-sections were taken of both the polyamide sample and a high temperature acrylate sample with the objective to gain further insight as to the cause of the slip (Figure 10(a)-(b)). Micrograph samples were cut using a diamond saw to conserve the properties at the cross-section. These samples were then mounted on Bakelite and polished using sandpaper and then fine grit disks, and then viewed on an optical microscope. The polyamide coated sample shows substantial deformation compared to that of the Acrylate, leading to a non-uniform coating. It is possible that the inconsistent coating distance effects the slip, or the slip may be a result of poor mechanical coupling between aluminum and polyamide in general. Further testing and the development of a model is required to fully understand this slippage.

Downloaded From: http://proceedings.spiedigitallibrary.org/ on 07/12/2017 Terms of Use: http://spiedigitallibrary.org/ss/termsofuse.aspx

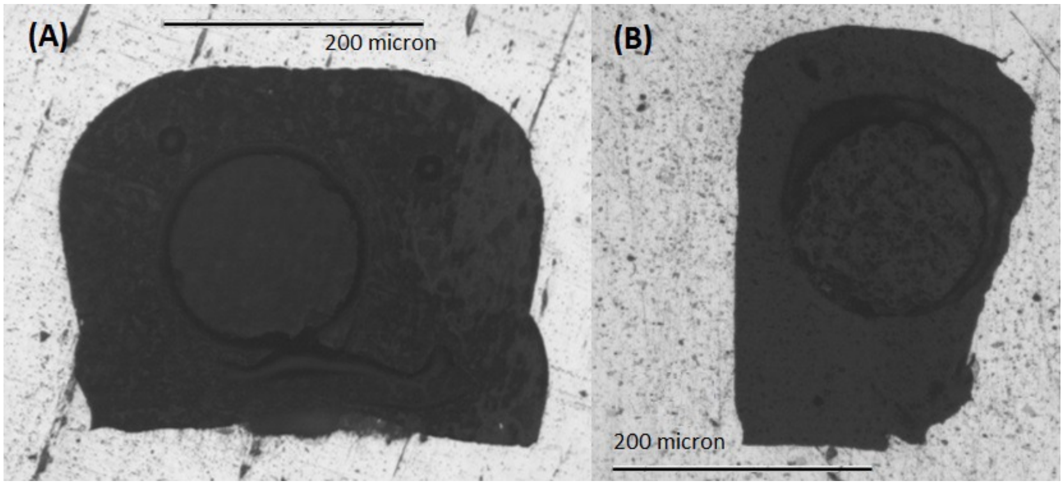

Figure 10. microscopy of tensile tested samples: (A) acrylate coated sample used in high temperature testing; (B) polyamide coated sample pulled to failure.

3.5 Thermal Characterization

Acrylate coated FBG sensors were chosen for high temperature characterization due to the lack of slip observed in room temperature tensile testing. FBG sensors showed no sign of inscription reversal, the shift in wavelength and reflectivity accelerated above the annealing temperature of the FBGs, during high temperature testing. This was confirmed by the fiber strain signal accurately tracking the modulus of elasticity of aluminum during testing up to 550 degrees Celsius. Despite the accurate modulus tracking, the samples were designed such that fiber ran through the length of the entire sample. This enforced mechanical coupling between the fiber in the grips of the load frame, well outside of the hot zone. High temperature test specimens have been designed with a curved configuration to address this issue (Figure 11).

Figure 11. high temperature test specimen. The Al-fiber matrix is only present in the hot zone due to the curved embedding configuration, allowing the fiber exit points to be present in the center of the sample rather than at the ends.

In order to examine the mechanical coupling between the sensor and the aluminum, a sample was thermally loaded while mechanically isolated in a lab oven. Figure 12 shows the apparent CTE of the FBG. The change in apparent CTE is due in part to the mismatch in CTE between silica glass, acrylate, and aluminum, and is also

Downloaded From: http://proceedings.spiedigitallibrary.org/ on 07/12/2017 Terms of Use: http://spiedigitallibrary.org/ss/termsofuse.aspx

a result of thermo-optic effects leading to changes in the index of refraction of the glass. At approximately 180 Celsius, the interrogator reached its maximum wavelength, and was unable to obtain higher strain measurements.

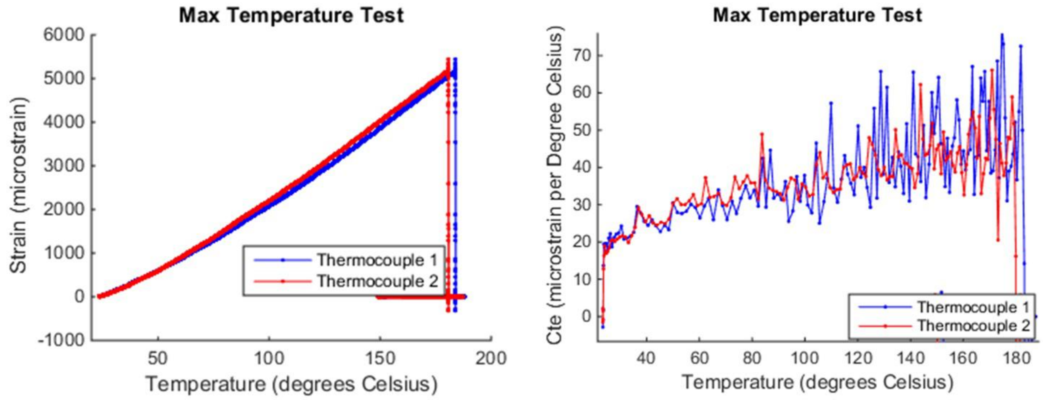

Figure 12. Acrylate coated sensor strain profile during mechanically unloaded heating.

4. CONCLUDING REMARKS

FBG sensors were embedded into aluminum test specimens through the UAM process. UAM was chosen for its ability to join metals, low process temperature, and integrated subtractive operations, which allow for the fabrication of smart metallic structures. The embedded FBG sensors were characterized by comparison to foil strain gages and determination of performance limits. Cantilever bending testing showed that the strain profiles between foil gages and FBGs matched, and tensile testing showed that the measured strain values were shared as well. Birefringence effects showed the need for an embedding channel prior to encapsulation in order to minimize cross-sectional deformation of the fiber, and no adverse effects were observed in the embedment of fiber into curved channels. High temperature testing showed no evidence of inscription reversal.

The high temperature tensile tests will be performed using the new sample configuration to ensure coupling only in the hot zone (Figure 11). This configuration is necessary as coupling was found to occur between the fiber and aluminum in the grips of the tensile test frame. FBG sensors with a lower nominal wavelength will also be used to redo the maximum temperature test with a greater range. Shaker testing will serve to provide more consistent data to use for analyzing the dynamic response of the FBG sensors. Cross-sections of additional samples will continue to provide insight into the interface interactions, and will drive a modeling effort into both the mechanical and thermal phenomena observed.

5. ACKNOWLEDGEMENTS

The authors wish to acknowledge the member organizations of the Smart Vehicle Concepts Center, a National Science Foundation Industry/University Cooperative Research Center established under grant IIP-1238286 (www.SmartVehicleCenter.org), and the technical and in-kind support from Insensys Ltd.

REFERENCES

[1] Pan, X., Liang, D., and Li, D., "Optical fiber sensor layer embedded in smart composite material and structure," *Smart materials and structures* **15**(5), 1231 (2006).

[2] Zhou, G. and Sim, L., "Damage detection and assessment in fibre-reinforced composite structures with embedded fibre optic sensors-review," *Smart Materials and Structures* **11**(6), 925 (2002).

[3] Huston, D., [*Structural sensing, health monitoring, and performance evaluation*], CRC Press (2010).

[4] Kashyap, R., [*Fiber Bragg Gratings*], Academic press (1999).

[5] Kuang, K. and Cantwell, W., "Use of conventional optical fibers and fiber Bragg gratings for damage detection in advanced composite structures: a review," *Applied Mechanics Reviews* **56**(5) (2003).

Downloaded From: http://proceedings.spiedigitallibrary.org/ on 07/12/2017 Terms of Use: http://spiedigitallibrary.org/ss/termsofuse.aspx

[6] Wong, K. V. and Hernandez, A., "A review of additive manufacturing," *ISRN Mechanical Engineering* (2012).
[7] Antreas Kantaros, D. K., "Fiber bragg grating based investigation of residual strains in abs parts fabricated by fused deposition modleing process," *Materials and Design* **50**(44) (2013).
[8] Maier, R. R., MacPherson, W. N., Barton, J. S., Carne, M., Swan, M., Sharma, J. N., Futter, S. K., Knox, D. A., Jones, B. J., and McCulloch, S., "Embedded Fiber Optic Sensors Within Additive Layer Manufactured Components," *IEEE Sensors Journal* **13**(3) (2013).
[9] Havermann, D., Mathew, J., MacPherson, W. N., Hand, D. P., and Maier, R. R., "Measuring residual stresses in metallic components manufactured with fibre bragg gratings embedded by selective laser melting," in [*International Conference on Optical Fibre Sensors (OFS24)*], 96340T–96340T, International Society for Optics and Photonics (2015).
[10] Graff, K., [*ASM Handbooks: Volume 6A, Welding Fundamentals and Processes*], American Society for Materials International (2011).
[11] Mou, C., Saffari, P., Li, D., Zhou, K., Zhang, L., Soar, R., and Bennion, I., "Smart structure sensors based on embedded fibre Bragg grating arrays in aluminium alloy matrix by ultrasonic consolidation," *Measurement Science and Technology* **20.3** (2009).
[12] Kong, C. Y. and Soar, R., "Method for embedding optical fibers in an aluminum matrix by ultrasonic consolidation," *Applied Optics* **44**(30) (2005).
[13] Standard, A., "E8/e8m. standard test methods for tension testing of metallic materials. west conshohocken (pa): Astm," International (2011).
[14] Wolcott, P., Hehr, A., and Dapino, M. J., "Optimized Welding Parameters of Al 6061 Ultrasonic Additive Manufactured Structures," *Journal of Materials Research* **29**(18) (2014).
[15] Agrawal, G. P., [*Fiber-optic communication systems*], vol. 222, John Wiley and Sons (2012).
[16] Katsunari Okamoto, T. H. and Edahiro, T., "Stress analysis of optical fibers by a finite element method," *IEEE Journal of Quantum Electronics* **17.10** (1981).

Downloaded From: http://proceedings.spiedigitallibrary.org/ on 07/12/2017 Terms of Use: http://spiedigitallibrary.org/ss/termsofuse.aspx